J Electroceram (2009) 23:536–541
DOI 10.1007/s10832-008-9530-2

Physical properties of transparent conducting indium doped zinc oxide thin films deposited by pulsed DC magnetron sputtering

Young Ran Park · Donggeun Jung · Ki-Chul Kim · Su Jeong Suh · Tae Seok Park · Young Sung Kim

Received: 28 May 2007 / Accepted: 18 June 2008 / Published online: 12 July 2008
© Springer Science + Business Media, LLC 2008

Abstract Transparent conducting In-doped (1at.%) zinc oxide (IZO) thin films are deposited on glass substrate by bipolar pulsed DC magnetron sputtering. We have investigated the effect of pulse frequency on the physical properties of the IZO films. A highly *c*-axis oriented IZO thin films were grown in perpendicular to the substrate. At optimal deposition conditions, IZO films with a smoothest surface roughness of ~3.6 nm, a low-resistivity of 5.8×10^{-3} Ωcm, and a high mobility of 14 cm/Vs were achieved. The optical spectra showed a high transmittance of above 85% in the UV–visible region and exhibited the absorption edge of near 350 nm. In micro-Raman, we observed the three phonon modes of host ZnO, which are E_2^{low}, E_2^{high}, and A_1 modes, and the three additional modes. The origin of three additional modes is attributed to the host lattice defect due to the effect of In dopant and increasing the pulse frequency.

Keywords Pulse DC magnetron sputtering · Semiconductor · In doped ZnO (IZO) · Transparent conducting oxide (TCO) · Raman spectra

Y. R. Park · D. Jung
Department of Physics, Institute of Basic Science and Center for Nanotubes and Nanocomposites, Sungkyunkwan University, Suwon 440-746, Korea

K.-C. Kim
Department of Design and Materials, Mokwon University, 21 Mokwongil, Seo-gu, Daejeon 302-318, Korea

S. J. Suh · T. S. Park · Y. S. Kim (✉)
Advanced Material Process of Information Technology, Sungkyunkwan University, Suwon 440-746, Korea
e-mail: youngsk@skku.edu

1 Introduction

ZnO is II–VI wide band gap semiconductor which has been extensively investigated for various applications such as transparent and conducting oxide (TCO) materials, surface acoustic wave (SAW) devices and optoelectronic devices. ZnO has a wide band gap of 3.3 eV, and UV emission resulting from a large exciton binding energy of 60 meV. Its band structure and optical properties are very similar to those of GaN, which is known to be a good material for the fabrication of optical devices such as light emitting devices (LED) or laser diodes (LD). Recently, ZnO can possibly be applied to serve as an alternate anode material to tin doped indium oxides (ITO) of TCO and demonstrate the available applications of plastic substrate with transparent anode. TCO films with unique characteristics of low resistivity and high transparency over the visible wavelength region have numerous applications in optoelectronic devices including thin film solar cell [1], organic light emitting devices (OLED) [2], and other flat panel displays (FPD) [3]. Recently, In or Al doped zinc oxide (IZO or AZO) films [4, 5] have been considered as possible alternatives to ITO films because ZnO thin films are more stable against hydrogen plasma, more abundant, and less expensive in comparison with the ITO films. ZnO-based films were deposited by several techniques such as RF sputtering process [6, 7], pulsed laser deposition (PLD) [8, 9], sol–gel method [10], and vacuum arc plasma evaporation (VAPE) [11]. Recently, bipolar pulsed DC magnetron sputtering process [12–18] has attracted notice as the deposition method of the industrially important coatings because it has higher deposition rate of defect-free ceramic films than RF magnetron sputtering process. These studies have shown that pulsing the magnetron discharge in the mid-frequency range (20–350 kHz) leads to increased plasma

densities and electron temperatures, and therefore, higher ion energy fluxes transported to the growing film, in comparison with continuous DC sputtering. Particularly, pulsed DC power as opposed to continuous DC power is used to prevent the formation of arcs [19–21].

There was a previous report on bipolar pulsed DC magnetron sputtering deposition of AZO thin films [12, 22–24]. However, reports on bipolar pulsed DC magnetron sputtering deposition of IZO thin films are hard to find. The correct selection of pulse parameters such as frequency, duty, and reverse voltage can result in extended arc-free operating conditions, and expect good physical properties of IZO films.

In the present work, IZO thin films were prepared on glass substrate by bipolar pulsed DC magnetron sputtering. The structural, optical, and electrical properties of the IZO films were investigated with various pulsed DC frequencies at constant duty cycle and discharge current. According to our knowledge, no detail Raman investigation of In doped ZnO have been reports yet. Therefore, we use nondestructive characterization such as micro-raman spectroscopy to study the effects of In substitution on the lattice dynamical properties of ZnO and identify the impurity phases.

2 Experimental details

IZO films were deposited on corning 7059 glass by asymmetrical bipolar pulsed DC magnetron sputtering. The targets were prepared by sintering the mixing 99.99% ZnO and In_2O_3 powders with In fraction of 1 at %. The sputtering chamber was pumped down to 1×10^6 Torr by turbo molecular pump and Ar gas was only used as a sputtering gas. The substrate to target distance, sputtering time, working pressure and pulsed DC power were kept at 7 cm, 15 min, 5 mTorr and 150 W, respectively. The pulsed frequency of DC power was varied in the 10–70 kHz at constant substrate temperature of 500°C. The thicknesses of the deposited films determined by the field emission scanning electron microscopy (FESEM) were in the 250±10 nm ranges.

The crystal structure, the electrical properties, the surface roughness, and the surface morphology of the deposited IZO films were investigated by X-ray diffraction (XRD) measurement, Hall-effect measurements using van der Pauw method, atomic force microscopy (AFM), and FESEM in the room temperature. The optical transmittance was recorded using an ultraviolet–visible spectrometer in the wavelength range of 200–1100 nm at room temperature and calculated the optical band gap energy. The micro-Raman measurement was performed in the backscattering geometry. The radiation of 514 nm from an Ar laser was focused to ~10 μm in diameter on the samples at room temperature.

3 Results and discussion

In Fig. 1, the crystalline structure and preferred orientation of the deposited films were investigated by XRD. ω-2θ scans of IZO thin films with the variation of pulse frequency are plotted. All patterns indicate the formation of the single wurzite-type ZnO phase. The ZnO related peaks in each pattern are shown in (0002) plane indicating a strong *c*-axis orientation. No evidence of In_2O_3 related phase was seen, confirming the monophasic nature of ZnO.

The *c*- and *a*-axis lattice constant, and the resultant unit cell volume of the IZO films, as estimated from the XRD data, are shown in Fig. 2(a). As the pulse frequency increases, the *c*- and *a*-axis lattice constant, and the resultant unit cell volume slightly increased. The estimated values of all films are larger than that of the pure ZnO (a=3.26 Å, c=5.21 Å, and V=143.85 Å). The estimated values can be interpreted in terms of the substitution of the In^{3+} by Zn^{2+} ions due to the larger ionic radii of In^{3+} ion (0.76Å) compared to Zn^{2+} ion (0.74 Å) [25]. The values increases with increasing the pulse frequency, which can be explained in terms of substitution by the larger In atoms increases lattice parameters *a* and *c* due to the intrinsic stress induced in the films.

In Fig. 2(b), the full-width at half-maximum (FWHM) from the (0002) peaks of IZO films with various pulse frequencies were measured by ω-2θ scan of XRD. When the pulse frequency of 30 kHz was applied to a target, the

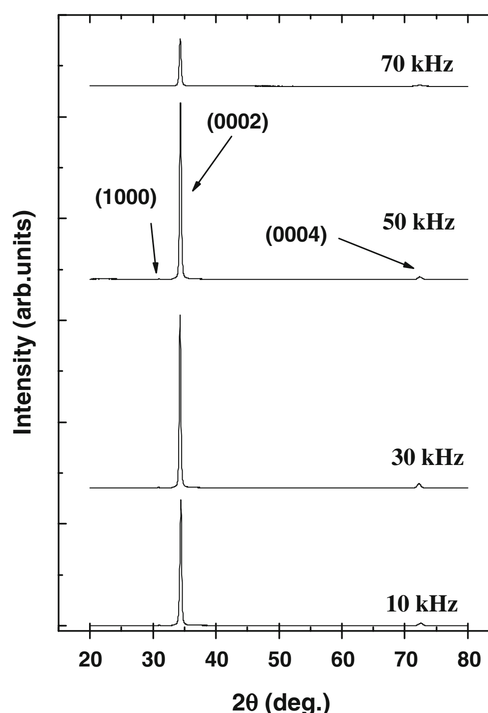

Fig. 1 XRD spectra of IZO films grown on glass substrate with pulse frequencies

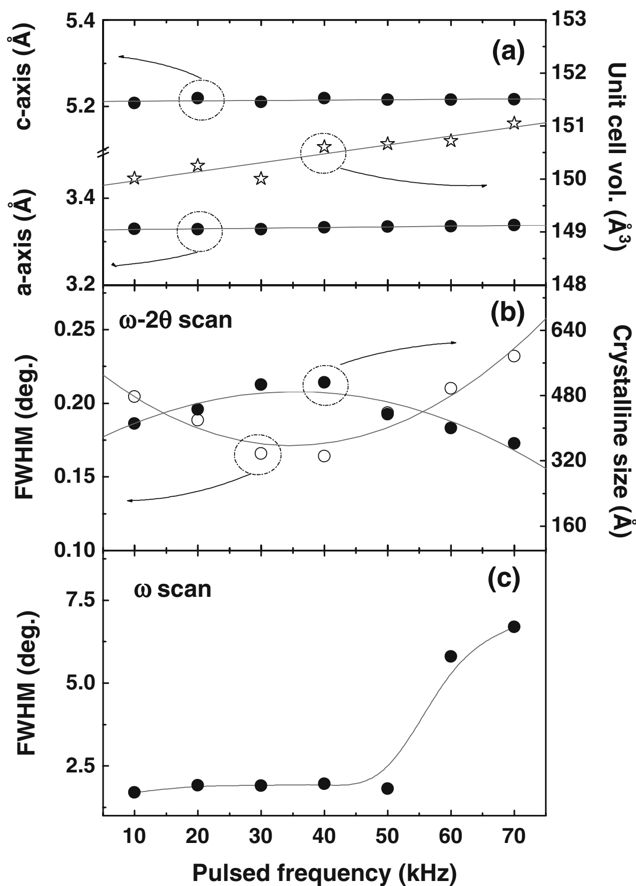

Fig. 2 Variation of the lattice constants and the resultant unit-cell volume of IZO films (**a**), the FWHM (0002) and crystalline size of IZO films in the ω-2θ scan (**b**), and the FWHM (0002) of IZO films in the ω scan (**c**) with pulse frequencies

peak intensity of (0002) plane showed the highest value. From the results of FWHM, the crystallite size of the IZO films was calculated by the using Scherer's equation. The value of FWHM appeared lowest value near the pulse frequency of 30 kHz and it increased at a pulse frequency higher than 50 kHz. As the value of FWHM is inversely proportional to the crystallite size, it implies that crystallite size in films increases with the increase pulse frequency up to 30 kHz. The increase of the crystallite size and the improvement of the crystallinity will be responsible for the decreasing the electrical resistivity due to diminishing in grain boundary scattering. The value of the crystallite size implies crystal information for the vertical direction rather than the lateral direction. All of the films exhibit the preferred (0002) orientation due to the minimal surface energy in the ZnO hexagonal wurtzite structure [26]. In Fig. 1, the XRD patterns show no diffraction from randomly oriented grains or impurity phases. This result indicates that the films are composed of a wurtzite type hexagonal structure and have a preferential orientation of *c*-axis normal to the substrate plane. It is well known that ZnO films consist of columnar grains grown with the *c*-axis orientation [27]. Therefore, this result indicates that the columnar-structured IZO thin films with vertical direction grown at pulse frequency of 30 kHz have highly *c*-axis crystallites to the substrate.

To estimate the preferred orientation of the grains in the thin film, the FWHMs of (0002) orientation were measured rocking curves by ω-scan. Figure 2(c) is a ω-scan of IZO films when the variation of the pulsed frequency was applied to a target. It is seen that FWHM of IZO films maintained about 1.9° up to 50 kHz pulsed frequency, but abruptly expanded for higher than 50 kHz. It indicates that grains in the film can be uniformly perpendicular to the glass surface at the optimal pulse frequency ranges. From the results, the IZO film will have random oriented grains at the pulse frequency of higher than 50 kHz.

To investigate the effect of pulse frequency on surface morphology and roughness of IZO films, SEM and AFM analysis were carried out. The surface morphology of the IZO films is shown in Fig. 3(a)–(d), which is found that the variation of the pulse frequency makes a significant influence on the surface morphology of the IZO films. The grain sizes show the largest when the pulse frequency of 30 kHz was applied and it decrease at a pulse frequency higher than 40 kHz. This is consisted with the crystallite size calculated from Scherrer's formula. When the pulse frequency of 30 kHz was applied, the crystalline size became the largest and the crystallinity was improved. Because the defects in grain boundaries along the *c*-axis preferred grain growth decreased and the surface of grains has greater kinetic energy to diffuse on the surface of the films. The surface roughness of the IZO films is analyzed by contact mode AFM analysis. Figure 3(e) shows that the films prepared at various pulse frequencies have different surface roughness. The surface roughness showed the largest root mean square (R_{RMS}) of 4.2 nm when the pulse frequency increased up to 20 kHz. The R_{RMS} of IZO films with the pulse frequency of higher than 30 kHz was less than 3.58 nm, which is similar to that of commercial ITO films. The decrease of the surface roughness can be explained in terms of the increase of conducting path in the films. As the surface roughness decreases, the effective surface area of films as well as the number of absorption sites for oxygen also decrease. These lead to the decrease of the resistivity and the improving the Hall mobility due to diminishing in grain boundary scattering [28].

Figure 4 shows the carrier concentration, Hall mobility, and electrical resistivity with variation of pulse frequency. The IZO films show n-type semiconductors in nature. In general, pure ZnO exhibits an n-type conductivity rising from the electrons in the conduction band. It has been widely considered that this n-type conductivity originated from the native defects such as oxygen vacancies(V_O) and

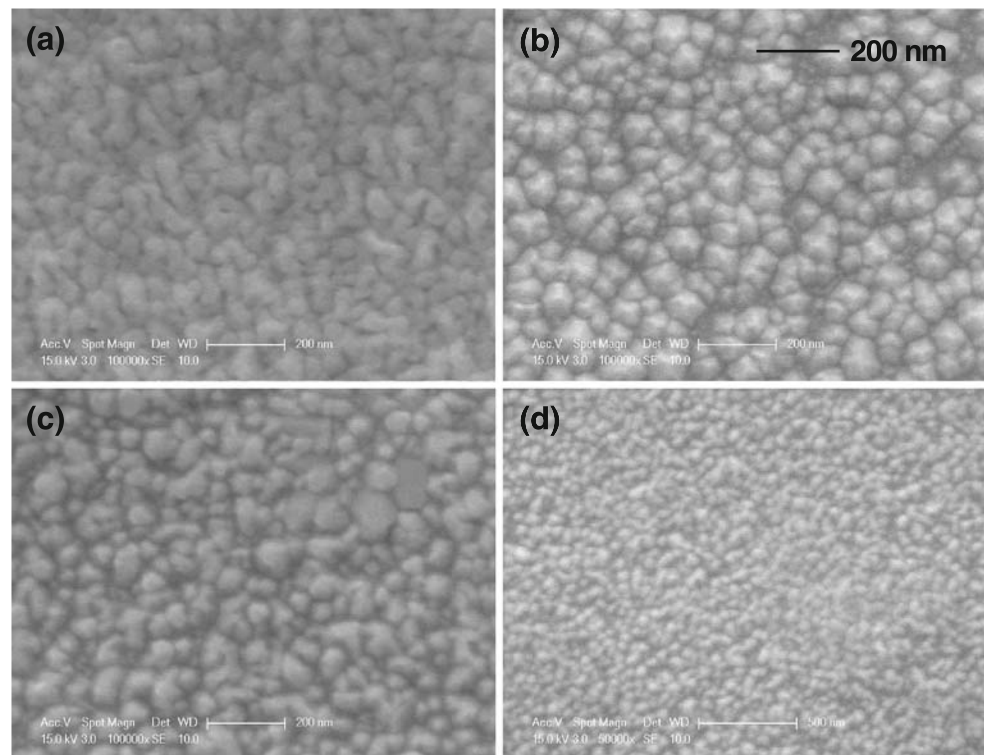

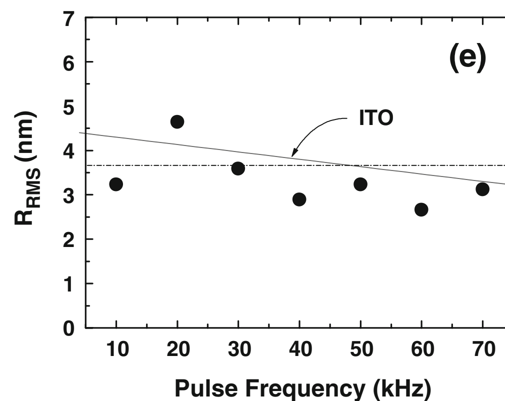

Fig. 3 SEM images on (**a**) 10 kHz, (**b**) 30 kHz, (**c**) 50 kHz, and (**d**) 70 kHz. (**e**) *RMS* surface roughness measured by AFM with pulse frequencies

zinc interstitials(Zn_i) [29, 30]. These defects in ZnO are easily ionized, and electrons produced by ionized defects contribute to the electrical conductivity. Thus, Zn_i and V_O play important roles in the ZnO film's electrical conductivity and act as donors in the crystal. Increasing the number of the native defects in the film gives rise to an increase in the carrier concentration and a decrease in the resistivity. On the other hand, the carrier concentration of IZO films is two order of magnitude higher than that of ZnO films. From this result, it shows that In impurity in ZnO films acts as an effective donor. The relatively higher carrier concentration indicates due to the concentration from In^{+3} ions on substitutional site of Zn^{+2} ions [6, 31, 32] as well as Zn_i and V_O [33]. The resources of carrier and the mobility was influenced by a few scattering mechanisms. In our study, it is found that the resistivity of IZO films is nearly constant with the variation of pulse frequency. It can be explained that carrier concentration was slightly changed from $6.7\times 10^{19}/cm^3$ to $8.4\times 10^{19}/cm^3$ and Hall mobility was varied from 12.0 cm^2/Vs to 15.0 cm^2/Vs. It is well known that higher charge carrier density will result in lower resistivity, but higher grain boundary scattering will cause higher resistivity. Additionally, it indicates that the decreased resistivity of films is attributed to the increase of the mobility. The mobility of carriers in these films can be interpreted mainly by the structural quality and surface roughness of the films due to the decrease of mobility is associated with the decrease of crystallite size and conducting path in the IZO films. Particularly, the increase of pulse frequency allows the sputtered atoms to move into more stable surface sites during deposition, which leads to the increase of crystallite size and the decrease of grain

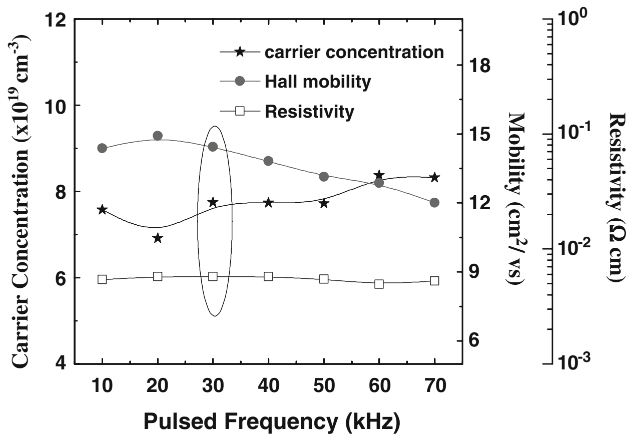

Fig. 4 Carrier concentration, mobility, and electrical resistivity of IZO film with pulse frequencies

boundary scattering due to charge carrier. It also allows the surface roughness of films to decrease [28]. This is the reason why the crystallinity of IZO films increases with the increase of pulse frequency till 30 kHz.

Figure 5 illustrates the optical transmission spectra of the IZO films at various pulsed frequencies and the resultant optical band gap energy shift as carrier concentration. *E(0)* and *E(n)* are optical band gap energy of pure ZnO and IZO, respectively. In the transmission spectra, the absorption edge was about 350 nm and optical transmittance was about 85~90% in the visible range. The optical absorption coefficient α is defined as $I=I_0e^{-\alpha d}$, where I is the intensity of transmitted light, I_0 is the intensity of incident light, and d is the thickness of the IZO film. In order to determine the E_0 of the optical band gap energy, square of the absorption coefficient α was plotted [34]. Extrapolation of the linear portion of α^2 to zero gives the value of the E_0. The excess carriers supplied by the impurities to the conduction band contribute to increase the electrical conductivity of ZnO. The conduction band edge is filled by excessive carriers

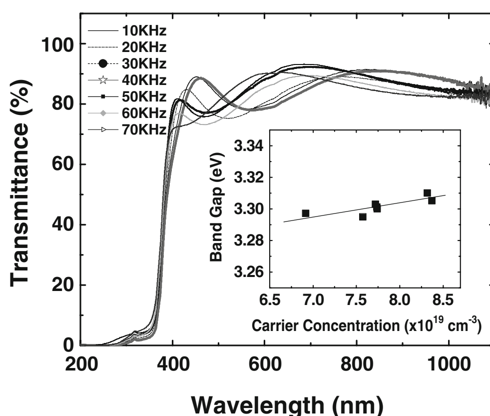

Fig. 5 Optical transmittance spectra of IZO films prepared with pulse frequencies and the insert is the evolution of E_0 energy shift of IZO with carrier concentration

donated by the impurities, known as the Burstein–Moss (BM) effect [35]. In our study, E_0 energy of IZO thin films is larger than that of pure ZnO and it is observed that the value of E_0 energy shift increases with increasing carrier concentration, which is consistent with BM effect.

In order to investigate, the effects of In dopant and pulse frequency on the lattice dynamical properties of ZnO thin films, micro Raman analysis was performed. Pure ZnO has a wurtzite structure and belongs to the $C_{6\nu}$ symmetry group. It will have one A_1, one E_1, two E_2 (high and low), and two B_1 optical phonon modes. The polar characteristics of the A_1 and E_1 modes are split into longitudinal (LO) and transverse optical (TO) components. Phonon modes of A_1 (~574 and ~380 cm^{-1}), E_1 (~583 and ~407 cm^{-1}), and E_2 (~101 and ~437 cm^{-1}) modes are Raman active, and the B_1 mode is silent at Raman spectra [36].

Figure 6 shows the micro-Raman spectrum of IZO thin film prepared at 500°C. Three phonon peaks of IZO at 95, 432, 573 cm^{-1} were observed and were assigned to the E_2^{low}, E_2^{high}, and A_1 modes of host ZnO. The additional mode at 271, 501, and 638 cm^{-1} have been observed. The broadening of the E_2^{low} and the decreasing intensity of the E_2^{high} phonon mode are mainly attributable to the damage and disorder induced by impurity doping [37, 38]. In the IZO film of 40 kHz, the increasing intensity of the A_1 phonon mode can be explained in terms of the defects due to O vacancies, Zn-interstitial defect states, or free carriers [39]. The origin of additional mode at 271 cm^{-1} is attributed to vibration of Zn atoms in the IZO film, where

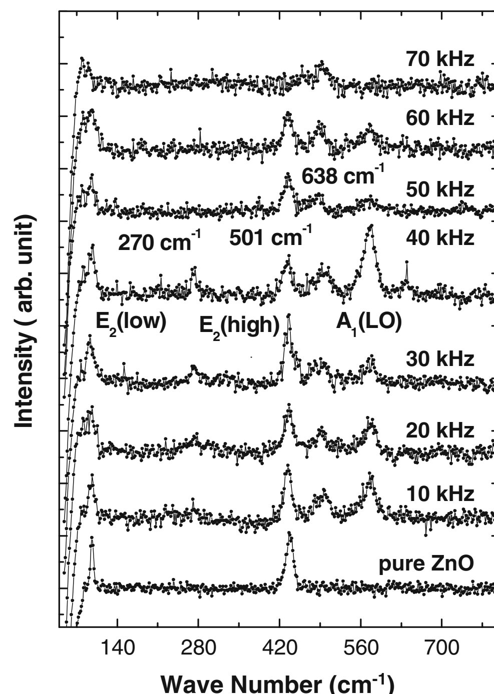

Fig. 6 Micro Raman spectra of IZO film when the variation of pulse frequency and the substrate temperature of 500°C were applied

parts of its first nearest neighbor O atoms are replaced by defect in the crystal lattice [40]. The other two additional modes arise from the optical phonon branch at the zone boundary induced by damage of the crystal lattice [40]. Therefore, the induced crystal damage in IZO thin film may be caused by host lattice defects such as vacancies and interstitials with increasing the pulse frequencies.

4 Conclusion

In this study, high quality, conductive, and highly transparent IZO films were deposited on glass substrate by pulsed DC magnetron sputtering technique in order to study the effects of various pulse frequency. At the optimal condition, IZO films with electrical resistivity of less than 5.8×10^{-3} Ωcm and optical transparency of higher than 85% in the visible wavelength region are achieved. The band gap energy increases with increase in carrier concentration which is attributed to Bustein–Moss shift. In dopant in the ZnO films exhibits the variation of the unit cell volume and crystalline quality, and we can also observe three additional raman vibration modes at 271, 501, and 638 cm^{-1} in the IZO films induced crystal damages with increasing the pulse frequencies higher than 40 kHz.

Acknowledgment This work was supported by the Korea Research Foundation Grant funded by the Korean Government (MOEHRD) (KRF-2005-005-J11902) and by the Ministry of Commerce, Industry, and Energy (MOCIE) through Advanced Material Process of Information Technology (AMPIT) (R12-2002-057-01001-0).

References

1. M. Kon, P.K. Song, Y. Shigesato, P. Frach, S. Ohno, K. Suzuki, Jpn. J. Appl. Phys **42**, 263 (2003). doi:10.1143/JJAP.42.263
2. S. Sohn, K. Park, D. Lee, D. Jung, H.M. Kim, U. Manna et al., Jpn. J. Appl. Phys **45**, 3733 (2006). doi:10.1143/JJAP.45.3733
3. Y. He, J. Kanicki, Appl. Phys. Lett **76**, 661 (2000). doi:10.1063/1.125854
4. J.J. Ho, C.Y. Chen, J. Electrochem. Soc **152**, G57 (2005). doi:10.1149/1.1829431
5. X.T. Hao, L.W. Tan, K.S. Ong, F. Zhu, J. Cryst. Growth **287**, 44 (2006). doi:10.1016/j.jcrysgro.2005.10.040
6. K.J. Kim, Y.R. Park, Appl. Phys. Lett **78**, 475 (2001). doi:10.1063/1.1342042
7. N. Jedrecy, H.J. Von Bardeleben, Y. Zheng, J.-L. Cantin, Phys. Rev. B **69**, 1 (2004). doi:10.1103/PhysRevB.69.041308
8. K. Yim, H. Kim, C. Lee, J. Electroceram **17**, 875 (2006). doi:10.1007/s10832-006-7036-3
9. M. Ohyama, H. Kozuka, T. Yoko, Thin Solid Films **306**(1), 78 (1997). doi:10.1016/S0040-6090(97)00231-9
10. A.C. Rastogi, S.B. Desu, P. Bhattacharya, R.S. Katiyar, J. Electroceram **13**, 345 (2004). doi:10.1007/s10832-004-5124-9
11. T. Minani, S. Ida, T. Miyata, Y. Minamoto, Thin Solid Films **445**, 268 (2003). doi:10.1016/S0040-6090(03)01159-3
12. P.J. Kelly, R.D. Arnell, Vacuum **56**, 159 (2000). doi:10.1016/S0042-207X(99)00189-X
13. S. Schiller, K. Goedicke, J. Reschke, V. Kirchhoff, S. Schneider, F. Milde, Surf. Coat. Technol **61**, 331 (1993). doi:10.1016/0257-8972(93)90248-M
14. S.M. Rossnagel, J.J. Cuomo, W.D. Westwood, *Handbook of Plasma Processing Technology* (Noyes, Park Ridge, NJ, 1990), p. 233
15. P. Frach, U. Heisig, C. Gottfied, H. Walde, Surf. Coat. Technol. **59**, 177 (1993). doi:10.1016/0257-8972(93)90079-4
16. P.J. Kelly, R.D. Arnell, J. Vac. Sci. Technol. A **16**, 2858 (1998). doi:10.1116/1.581432
17. P.J. Kelly, R.D. Arnell, J. Vac. Sci. Technol. A **17**, 945 (1999). doi:10.1116/1.581669
18. A. Belkind, A. Freilich, R. Scholl, Surf. Coat. Technol. **108–109**, 558 (1998). doi:10.1016/S0257-8972(98)00635-5
19. J.W. Bradley, H. Baecker, P.J. Kelly, R.D. Arnell, Surf. Coat. Technol. **135**, 221 (2001). doi:10.1016/S0257-8972(00)00990-7
20. J.W. Bradley, H. Baecker, P.J. Kelly, R.D. Arnell, Surf. Coat. Technol. **142–144**, 337 (2001)
21. J.W. Bradley, H. Baecker, Y. Arando-Gonzalvo, P.J. Kelly, R.D. Arnell, Plasma Sources Sci. Technol **11**, 165 (2002). doi:10.1088/0963-0252/11/2/307
22. C. Guillén, J. Herrero, Vacuum **82**, 668 (2008). doi:10.1016/j.vacuum.2007.10.013
23. P.J. Kelly, Y. Zhou, A. Postill, Thin Solid Films **426**, 111 (2003). doi:10.1016/S0040-6090(02)01332-9
24. V. Sittinger, F. Ruske, W. Werner, C. Jacobs, B. Szyszka, D.J. Christie, Thin Solid Films (2007). doi:10.1016/j.tsf.2007.10.031
25. R.D. Shannon, Acta Crystallogr. A **32**, 751 (1976). doi:10.1107/S0567739476001551
26. J.F. Chang, H.L. Wang, M.H. Hon, J. Cryst. Growth **211**, 93 (2000). doi:10.1016/S0022-0248(99)00779-4
27. X. Jiang, C.L. Jia, B. Szyszka, Appl. Phys. Lett **80**, 3090 (2002). doi:10.1063/1.1473683
28. E.G. Fu, D.M. Zhuang, G. Zhang, M. Zhao, W.-F. Yang, J.-F. Liu, Microelectron. J **35**, 383 (2004). doi:10.1016/S0026-2692(03)00251-9
29. S.Y. Lee, Y. Li, J.S. Lee, J.K. Lee, M. Nastasi, S.A. Crooker et al., Appl. Phys. Lett **85**, 218 (2003). doi:10.1063/1.1771810
30. H.S. Kang, J.S. Kang, J.W. Kim, S.Y. Lee, J. Appl. Phys **95**, 1246 (2004). doi:10.1063/1.1633343
31. Y.M. Hu, C.W. Lin, J.C.A. Huang, Thin Solid Films **497**, 130 (2006). doi:10.1016/j.tsf.2005.10.058
32. T. Minami, H. Sato, H. Nanto, S. Takata, Jpn. J. Appl. Phys **24** (10), L781 (1985). doi:10.1143/JJAP.24.L781
33. R. AlAsmar, S. Juillaguet, M. Ramonda, A. Giani, P. Combette, A. Khoury et al., J. Cryst. Growth **275**, 512 (2005). doi:10.1016/j.jcrysgro.2004.12.034
34. R.A. Smith, *Semiconductors* (Cambridge University, Cambridge, 1968), p. 189
35. E. Burstein, Phys. Rev **93**, 632 (1954). doi:10.1103/PhysRev.93.632
36. N. Ashkenov, B.N. Mbenkum, C. Bundesmann, V. Riede, M. Lorenz, D. Spemann et al., J. Appl. Phys **93**, 126 (2003). doi:10.1063/1.1526935
37. K. Samanta, P. Bhattacharya, R.S. Katiyar, W. Iwamoto, P.G. Pagliuso, C. Rettori, Phys. Rev. B **73**, 245213 (2006). doi:10.1103/PhysRevB.73.245213
38. W.B. Mi, H.L. Bai, H. Liu, C.Q. Sun, J. Appl. Phys **101**, 023904 (2007). doi:10.1063/1.2426377
39. J. Alaria, M. Bouloudenine, G. Schmerber, S. Colis, A. Dinia, P. Turek, M. Bernard, J. Appl. Phys **99**, 08M118 (2006)
40. J.B. Wang, H.M. Zhong, Z.F. Li, W. Lua, Appl. Phys. Lett **88**, 101913 (2006). doi:10.1063/1.2185261